ANALYTICAL MODELING OF PLASMA EFFECTS ON PECVD-GROWN GRAPHENE-HYBRID SUPERCAPACITOR PERFORMANCE

THESIS

SUBMITTED IN PARTIAL FULFILLMENT OF THE REQUIREMENTS FOR THE AWARD OF THE DEGREE

OF

MASTERS OF SCIENCE
IN
PHYSICS

Submitted by:
SUBHAJEET KUNDU
24/MSCPHY/55

Under the supervision of
Prof. SURESH C. SHARMA

DEPARTMENT OF APPLIED PHYSICS

DELHI TECHNOLOGICAL UNIVERSITY

(Formerly Delhi College of Engineering)

Bawana Road, Delhi – 110042

May, 2026

DEPARTMENT OF APPLIED PHYSICS

DELHI TECHNOLOGICAL UNIVERSITY

(Formerly Delhi College of Engineering)

Bawana road, Delhi – 110042

CANDIDATE'S DECLARATION

I, SUBHAJEET KUNDU, Roll No. 24/MSCPHY/55, student of M.Sc. Physics (Department of Applied Physics), hereby declare that the thesis presented in MSPH-210 Dissertation-II, titled "ANALYTICAL MODELING OF PLASMA EFFECTS ON PECVD-GROWN GRAPHENE-HYBRID SUPERCAPACITOR PERFORMANCE", in partial fulfilment of the requirements for the award of the degree of Master of Science, submitted to the Department of Applied Physics, Delhi Technological University, is an authentic record of my own work carried out during the period from February 2025 to May 2026 under the supervision of Prof. Suresh C. Sharma, Department of Applied Physics, Delhi Technological University.

The work has been communicated in a peer-reviewed journal, with the following details:

- **Title of the Paper:** Analytical Modeling of Plasma Effects on PECVD-Grown Graphene-Hybrid Supercapacitor Performance
- **Manuscript Number:** EST-D-26-05966
- **Author Names:** Subhajeet Kundu and Suresh C. Sharma
- **Status of Paper:** Submitted on 17 April 2026 and currently showing "Required Reviews Completed" as of 26 May 2026.

Place: Delhi

Date: 29/05/2026 **Subhajeet Kundu**

This is to certify that the student has incorporated all the corrections suggested by the examiners in the thesis and that the statement made by the candidate is correct to the best of my knowledge.

Prof. Suresh C. Sharma

DEPARTMENT OF APPLIED PHYSICS
DELHI TECHNOLOGICAL UNIVERSITY
(Formerly Delhi College of Engineering)
Bawana Road, Delhi-110042

CERTIFICATE

I hereby certify that the Project Dissertation titled "ANALYTICAL MODELING OF PLASMA EFFECTS ON PECVD-GROWN GRAPHENE-HYBRID SUPERCAPACITOR PERFORMANCE" which is submitted by SUBHAJEET KUNDU, Roll No. 24/MSCPHY/55, Department of Applied Physics, Delhi Technological University, Delhi in partial fulfilment of the requirement for the award of the degree of Master of Science, is a record of the project work carried out by the student under my supervision. To the best of my knowledge this work has not been submitted in part or full for any Degree or Diploma to this University or elsewhere.

Place: Delhi
Date: 29.05.2026

Prof. SURESH C. SHARMA
SUPERVISOR

DEPARTMENT OF APPLIED PHYSICS
DELHI TECHNOLOGICAL UNIVERSITY
(Formerly Delhi College of Engineering)
Bawana Road, Delhi-110042

ACKNOWLEDGEMENTS

I would like to express my deepest sincere gratitude to my supervisor, Prof. Suresh C. Sharma, Professor, Department of Applied Physics, Delhi Technological University for giving me the opportunity to work under his guidance and for constant inspiration and incessant support throughout the project. I take this opportunity to express indebtedness to my supervisor for his enthusiastic help, his expertise, brilliant ideas, valuable suggestions, and constant encouragement. I am grateful to acknowledge the constant help and convenience at every step of the project by all the lab members (Ph.D. scholars), Dept. of Applied Physics. Lastly, I am thankful to my family and friends for their love, care, and support who patiently extended all sorts of help for accomplishing this task.

SUBHAJEET KUNDU
(24/MSCPHY/55)

ABSTRACT

We develop an analytical framework to examine how plasma parameters influence electrode formation and, consequently, device performance. Although plasma-enhanced chemical vapor deposition (PECVD) technique is widely used for graphene electrode synthesis, quantitative relations between plasma parameters and supercapacitor performance remain limited. In this work, fundamental of plasma parameters, including electron density, electron temperature, Debye screening length, and sheath-related ion dynamics are incorporated into an analytical model that describes plasma-surface interactions during electrode formation. A roughness factor driven by ion bombardment is derived to correlate the plasma conditions with the electrochemical surface accessibility. The resulting increase in effective surface area directly influences both the double layer and pseudo-capacitance charge storage mechanisms, which describe the key device performance parameters such as specific capacitance, energy density, and power density. These calculations are performed using a Python-based simulation under varying plasma conditions. The electron density is varied over the range of 10^{15}-10^{17} m^{-3}, while the electron temperature is limited to 1-5 eV to reflect typical PECVD conditions. The results show that increasing the plasma density enhances the ion flux to the electrode surface, which enhances surface roughness and increases the effective electrode area, leading to improved energy storage capability. However, electron temperature influences capacitance through competing mechanisms. While increased Debye length weakens electrostatic coupling, the simultaneous increase in ion velocity enhances ion-flux and surface roughness, resulting in a non-monotonic dependence. These trends align with previously reported energy storage improvements in graphene-based hybrid supercapacitors, showing that plasma conditions can control energy storage performance, thereby providing a physically grounded model for predicting energy storage trends under varying plasma conditions.

Keywords: PECVD, plasma parameters, plasma-surface interactions, graphene-hybrid supercapacitors.

CONTENTS

LIST OF FIGURES

LIST OF TABLES

LIST OF SYMBOLS AND ABBREVIATIONS

Symbol / Abbreviation	Full Form
PECVD	Plasma-Enhanced Chemical Vapor Deposition
EDLC	Electric Double Layer Capacitor
HSC	Hybrid Supercapacitor
VAG	Vertically Aligned Graphene
VGS	Vertical Graphene Sheets
ESR	Equivalent Series Resistance
BET	Brunauer-Emmett-Teller
RF	Radio Frequency
IEDF	Ion Energy Distribution Function
MXene	Two-dimensional Transition Metal Carbide/Nitride
C_{EDL}	Electric Double Layer Capacitance
C_{pseudo}	Pseudo-capacitance
C_{total}	Total Capacitance
C_{sp}	Specific Capacitance
E_{device}	Device-Level Energy Density
P_{max}	Maximum Power Density

Symbol / Abbreviation	Full Form
λ_D	Debye Length
v_B	Bohm Velocity
Γ_i	Ion Flux
Φ_i	Ion Fluence
R_f	Surface Roughness Factor
Γ_s	Electrochemically Active Site Density
n_e	Electron Density
T_e	Electron Temperature
m_i	Ion Mass
ε_0	Permittivity of Free Space
ε_r	Relative Permittivity
k_B	Boltzmann Constant
e	Elementary Charge
F	Faraday Constant
R	Universal Gas Constant
T	Operating Temperature
A_{eff}	Effective Surface Area

CHAPTER-1

INTRODUCTION AND OBJECTIVES

1.1 Background and Motivation

The rapid expansion of portable electronics, electric vehicles, and grid-scale renewable energy systems has created an exceptional demand for electrochemical energy storage technologies that can simultaneously deliver high energy capacity, high power output, rapid charge-discharge cycling, and extended operational lifetimes. Conventional energy storage devices fall into two broad functional categories: rechargeable batteries, which offer high energy density through bulk faradaic electrochemical reactions, and conventional electrochemical double-layer capacitors, which offer exceptional power density and cycling stability through fast, reversible electrostatic charge storage at the electrode surface [1].

Supercapacitors, also referred to as ultracapacitors or electrochemical capacitors, occupy a unique and strategically important position in the energy storage landscape. Through electrostatic ion adsorption at the electrode-electrolyte interface-a mechanism that avoids the slow solid-state diffusion characteristic of battery electrodes-supercapacitors are capable of delivering energy bursts at rates several orders of magnitude faster than batteries, while also sustaining hundreds of thousands of charge-discharge cycles without significant capacity degradation [1, 2]. For these reasons, these devices are especially suitable for use in situations that require quick energy delivery and uptake, like in regenerative braking of electric vehicles, in load-leveling systems of renewable energy sources, and in pulse power applications in industry.

Unfortunately, the energy density of traditional supercapacitors, ranging from 3 to 10 Wh/kg, is significantly smaller compared to that of lithium-ion batteries, which is 100-200 Wh/kg, which greatly reduces their potential as efficient stand-alone energy storage devices [18].

Hybrid supercapacitors (HSCs) could be seen as an innovative approach to tackling this problem. HSCs are designed by adding the second electrode to a typical supercapacitor made of a high specific surface area carbon-based material, which provides electrostatic energy storage; this electrode enables fast faradaic redox reactions at its surface and thus allows harnessing of both electrostatic and faradaic energies [3].

Graphene stands out as one of the most promising material candidates for use in electrode construction for HSCs based on its exceptional combination of physical characteristics. In fact, graphene may be described as a 2D allotrope of carbon composed of a monolayer of sp2-hybridized carbon atoms arranged in a honeycomb structure. It has a theoretical specific surface area of 2630 $m^2\ g^{-1}$ [4], nearly metallic conductivity, excellent mechanical flexibility and strength [5], as well as notable chemical resistance to various electrochemical processes. Altogether, these properties make graphene an optimal material for use in electrodes of HSCs.

Unfortunately, despite all the above-described benefits of graphene, its performance as an electrode material remains far from perfect in terms of its actual electrochemical capabilities. Namely, the main problem associated with the employment of graphene in electrodes is the self-stacking of graphene sheets due to van der Waals interactions between them, thus reducing the available electrode surface area and hindering the penetration of electrolyte ions into the material's interior. As a result, the specific capacitance of actual graphene electrodes amounts to about 100-400 $F\ g^{-1}$, much lower than the theoretically achievable value of around 550

$F\ g^{-1}$ [4].

1.2 Graphene-Based Hybrid Supercapacitors

Two general approaches have been proposed to date in the literature to address the limitations associated with pristine graphene electrodes in terms of energy storage performances. The first approach consists of engineering the graphene matrix architecture, which includes

incorporating in-plane porosity in the structure (holey graphene), or building three-dimensional interconnected structures as well as hierarchical porous structures to improve ion diffusion and ensure high surface accessibility. Xu et al. [6] showed that by introducing porosity into the graphene scaffolds, which is achieved via selective etching of the graphene basal plane, additional edges can be formed and short ion transfer channels are created, leading to improved capacitance performances.

On the other hand, the second approach consists of adding redox active secondary species into the graphene matrices as pseudocapacitive materials to facilitate pseudocapacitive charging. Transition metal oxide compounds such as manganese dioxide (MnO_2), ruthenium oxide (RuO_2), and iron oxide (Fe_3O_4) are some of the well-studied pseudocapacitive materials to date. Their ability to perform rapid and reversible surface redox reactions enables the development of highly efficient pseudocapacitances that can substantially increase the overall charge storage compared to those solely based on physical adsorption. Another group of pseudocapacitive compounds includes two-dimensional MXene materials, which refer to transition metal carbides and nitrides [7].

Successful fabrication of highly effective graphene-based HSCs in terms of electrode performance, irrespective of the particular hybrid configuration used, critically hinges on the quality of the electrode surface. Surface characteristics such as roughness, porosity, density of defects, surface functional group chemistry, and access to electrochemical activity of the electrode surface all determine the electrode's ability to store charge. These considerations have contributed to the increased focus on modifying the electrode surface properties once they are fabricated.

1.3 Graphene as a promising electrode material

Graphene has emerged as one of the most promising materials for supercapacitor electrodes due to its exceptional properties:

- High specific surface area (~2630 m^2/g), enhancing capacitance
- Atomic-scale thickness, maximizing ion access and minimizing diffusion path
- High electrical and thermal conductivity, enabling fast charge-discharge cycles
- Mechanical strength and flexibility, offering superior cycle stability
- Chemical stability, resistant to oxidation and electrolyte corrosion

Graphene's two-dimensional structure allows for the formation of vertically aligned graphene (VAG) or graphene nanowalls, which further enhance electrolyte access, reduce ion diffusion paths, and increase electrochemical activity.

1.3.1 Plasma-Enhanced Chemical Vapor Deposition (PECVD)

It is safe to say that plasma enhanced chemical vapor deposition (PECVD) has become one of the most promising approaches not only for preparing but also modifying the surfaces of graphene-based electrodes. In PECVD reactors, plasma, which is ionized at low density in an inert gas such as argon or in gas mixtures with reactive components such as hydrogen, nitrogen, or carbon sources, provides reactive radicals and energetic ions, enabling material deposition, surface etching, and/or chemical modification of surface properties, depending on processing conditions [8, 9].

Unlike thermal CVD methods, PECVD makes it possible to reduce the temperature of the substrates involved and have better control over the processes of modification of the graphene surfaces by altering the plasma parameters. Energetic ions provided by PECVD may break carbon-carbon bonding on the surface of the basal plane of graphene, creating defect sites,

roughening its surface, introducing hydroxyl, carboxyl, and epoxy functional groups, and making it hydrophilic [8, 11, 12].

The key aspect setting apart plasma enhanced chemical vapor deposition (PECVD) from other methods for surface modification lies in the high level of controllability provided by plasma processing parameters such as electron density (ne) and electron temperature (Te). These parameters affect ion flux to the substrate, energy of impacting ions, radical generation, and extent of plasma-surface interaction. Previous experiments and theory have shown that electron density and electron temperature have direct effects on surface morphology in plasma treated electrodes and, as a result, affect the electrochemistry of these surfaces [9, 12]. Indeed, in their work on modeling the interaction between plasma and carbon nanomaterials, Sharma and Gupta [9] developed some basic connections between the physics of these processes and surface modification phenomena observed in electrochemistry.

Though the positive effect of PECVD on electrode behavior can be clearly seen in the previous research, most of the literature on the subject focuses on experimental results obtained in a trial-and-error fashion based on optimization of plasma processing conditions. In contrast, quantitative models connecting plasma parameters to electrode characteristics and, as a result, electrochemical performance are rather rare. This is precisely why modeling efforts aimed at filling the gap described above became the focus of this work.

1.4 Research Objectives

The general aim of this thesis is to construct and validate a complete analytical model which would enable quantification of correlations between PECVD plasma properties and electrochemical performances of graphene-based hybrid supercapacitors. These aims will be achieved by completing the following sub-tasks:

- Derivation of analytical expressions for major parameters associated with plasma-surface interaction-Debye length, Bohm velocity, ion flux, and ion fluence-in PECVD process based on argon plasmas.

- Derivation of surface evolution model connecting ion fluence with surface roughness and density of electrochemically active sites, taking into account the respective saturation effect.

- Conducting development of analytical models describing electrochemical capacitance of EDLC and pseudocapacitance contribution to overall capacitive behavior of HSC electrode, where each of these contributions is linked with plasma-related surface changes.

- Assessment of sensitivity of such parameters as specific capacitance, energy and power densities, and Ragone plots with respect to variation in plasma electron density and electron temperature.

- Validation of obtained theoretical results with the help of experimentally reported parameters of graphene-based HSCs.

1.5 Thesis Organization

Structure of the remaining sections of this thesis is described below. In chapter 2, an extensive literature review is carried out with respect to the history of development of supercapacitor technology, fabrication of graphene electrodes, physics of interactions between the plasma and its target surface, and previous models of electrochemical capacitor. Chapter 3 deals with the theoretical background and equation governing the analytical model involving plasma parameters, surface morphological features, and electrochemical capacitance modeling. In chapter 4, simulation results and their discussions on capacitance behavior, specific

capacitance, energy density, power density, and Ragone plot under different plasma parameters are given. The final chapter will provide conclusions drawn from this research work and limitations in the current model and future directions of research.

CHAPTER-2

LITERATURE REVIEW

2.1 Fundamentals of Electrochemical Capacitors

The science and engineering behind electrochemical capacitors have been developed based on pioneering work done by Conway et al., whose textbook Electrochemical Supercapacitors [2] is now considered the authoritative source in the field. The theory developed by Conway et al. recognizes that there are two types of charge storage mechanism, namely the electrostatic adsorption of ions from the electrolyte at the electrode/electrolyte interface leading to an electric double-layered capacitance, and rapid and reversible faradaic reactions taking place exclusively within the electrode or near-surface area, leading to pseudo-capacitance.

An electric double layer develops when electronic charge is separated from ionic charge in an interface between an electrode and electrolyte. The earliest model used to describe such an interface is the Helmholtz theory, where the interface is described as a parallel-plate capacitor having a fixed distance between plates equal to the size of solvated ions. While the Helmholtz theory provides an understanding of the double layer structure, it does not offer a comprehensive treatment of it, unlike theories such as the Gouy-Chapman and Stern models, which give a much better understanding of the double-layer interface especially at varying concentrations and potentials [2, 17].

The pseudo-capacitance effect, in comparison, stems from electrochemical reactions that create charges related to the potential, but fundamentally follow a faradaic reaction type. Such reactions can include underpotential deposition, surface redox reactions of transition metal oxides and conducting polymers, and ion intercalation into host materials that form layers [2]. The Langmuir adsorption isotherm serves as a theoretical approach to describe surface redox pseudo-capacitance by regarding electrochemically active sites as a finite set of independent adsorption sites of the electrode material [2, 18].

The study of Wang et al. [1] gives a detailed overview of electrode materials for electrochemical supercapacitors, listing all key features of different carbon-based materials, metal oxides, and conducting polymers under different electrolyte conditions. This review provides a basis for understanding the overall trends in electrochemical supercapacitors before the development of graphene materials. It also underscores the importance of surface area, electrical conductivity, and electrochemical stability as key properties determining the supercapacitor performance.

2.2 Evolution of Graphene-Based Electrode Materials

Demonstration of graphene supercapacitor electrodes experimentally was demonstrated by Stoller et al. [4], which showed that chemically reduced graphene oxide can provide about 135 F g^{-1} specific capacitance in aqueous electrolytes and 99 F g^{-1} in organic electrolyte. However, the values of capacitance obtained were significantly below the theoretically possible. Nevertheless, the study provided the essential proof of principle for using graphene as a supercapacitor material, which triggered an enormous body of research trying to enhance its electrochemical characteristics.

One of the key points discovered after the initial studies was the strong impact that the ability to access the graphene surface had on the electrochemical properties of the latter. Although theoretically graphene should possess extremely high surface area, in reality due to restacking of the layers the electrochemically active surface area of graphene becomes substantially reduced. To overcome this problem several approaches have been devised, including introduction of a spacer layer to prevent graphene layer from contacting, manufacturing of three-dimensional structures like graphene foam and aerogels, and creation of pores inside the structure of the material [6].

Xu et al. [6] reported an increase in specific capacitance and rate capability in holey graphene structures produced via controlled etching, which was related to the combined effects of larger accessible surface areas, reduced ion diffusion distances, and increased edge defects. These observations highlight the significance of both morphology and defect engineering in the development of effective graphene electrodes.

A wealth of research has been conducted on the incorporation of pseudocapacitive materials in graphene electrodes in order to overcome the constraints associated with purely EDLC-type capacitors. Of the various pseudocapacitive materials researched thus far, MnO_2 has been one of the most extensively investigated. This stems from the high theoretical capacitance of MnO_2, its abundant and eco-friendly nature. Toupin et al. [21] laid down valuable insights regarding the charge storage mechanism of MnO_2 in aqueous electrolyte systems; pseudocapacitance in this case is a result of facile adsorption/intercalation of alkali metal cations into the material structure with subsequent change in manganese oxidation states. The determination of active site density of the MnO_2-graphene electrodes is critical for modeling and will be used herein as a point of comparison [21].

In recent years, there has been much development on the use of MXene-graphene based composites for energy storage devices. The research by K et al. [7] documented the synthesis methods, energy storage mechanism, and electrochemical properties of the MXene-carbon hybrid systems, focusing on the mutual enhancement resulting from the combination of their high conductivity and surface redox activity of MXenes with the structural versatility and surface area of graphene-based supports.

Comprehensive performance benchmarking for graphene-based supercapacitors and HSCs was provided by Rani et al. [23], who reported ultra-high energy density values for MnO_2/reduced graphene oxide hybrid nanoscroll architectures, and by Wang et al. [22], who systematically

characterized the performance of graphene-based supercapacitor devices. These studies provide the experimental reference data against which the analytical model developed in this thesis is validated.

2.3 Plasma Treatment for Graphene Electrode Functionalization

The use of plasma treatment to modify the surface properties of carbon-based electrode materials has been the subject of growing investigation over the past decade. Plasma exposure can introduce a range of surface modifications depending on the plasma chemistry, power, pressure, and exposure duration, including the creation of structural defects, the introduction of surface functional groups, the modification of surface wettability, and the generation of porous surface features through selective etching [8, 12].

Meng et al. [11] reported a systematic investigation of plasma treatment effects on graphene fiber-based supercapacitor electrodes. Their findings demonstrated that plasma exposure significantly enhances the electrochemical performance of graphene fibers through a combination of increased surface area, improved electrolyte accessibility, and the generation of electrochemically active defect sites. Specifically, they observed that plasma treatment increases the Brunauer-Emmett-Teller (BET) surface area of graphene fibers by factors of 10-20 relative to untreated samples, consistent with the saturation limits for the roughness factor adopted in the present analytical model. Plasma-treated graphene fiber electrode specific capacitances in the region 100-400 F/g were demonstrated by other researchers, offering key experimental confirmation of results obtained from the theoretical framework presented here.

In a seminal work, Wang et al. [12] offered an extensive review on the use of plasmas to synthesize and functionalize advanced electrochemical energy storage materials. The study includes discussion on a wide range of plasma treatments-from plasma-induced defect engineering, surface functionalization, nano structuring, to composite material synthesis-and

systematically analyzes the influence of plasma parameters on the resulting surface properties. Importantly, the study also examines the conflictive effects of defect creation vs. physical damage due to high ion fluences, offering the theoretical foundation of the saturation phenomenon modeled in this thesis. The authors' calculations of ion bombardment cross sections in graphitic carbons directly validate the roughening coefficient used in the proposed surface roughness/active sites modeling approach.

The mechanisms underlying radiation damage processes caused by ion beam irradiation on carbon nanostructures have been thoroughly investigated by Banhart [13] whose extensive review on the effects of irradiation on carbon nanostructures continues to serve as a cornerstone for studying ion–graphene interactions. Banhart's analysis of displacement cross-sections for ion bombardment of graphitic carbon-covering a range of ion masses and energies relevant to PECVD conditions-directly informed the selection of the roughening coefficient ($\alpha = 10^{-20}$ m²) adopted in the present model.

Ghanashyam and Jeong [15, 16] investigated the synthesis and electrochemical characterization of plasma-treated nitrogen-doped graphite oxide and carbon nanofiber electrodes for supercapacitor applications. Their results demonstrated that plasma treatment of nitrogen-doped carbon materials significantly enhances specific capacitance, attributing the improvement to the combined effects of increased active surface area, enhanced nitrogen content, and the generation of additional redox-active surface sites. Specific capacitance values of up to 900 F g^{-1} reported in these studies represent the upper bound of the range against which the present model is validated.

Joseph and Shanov [8] reported the fabrication and electrochemical characterization of symmetric supercapacitors based on nitrogen-doped and plasma-functionalized three-dimensional graphene. Their study provides direct experimental evidence that plasma

functionalization can simultaneously increase surface area and introduce electrochemically active nitrogen functional groups, with both effects contributing to enhanced capacitance. The plasma exposure time of 10 s adopted in the present model is consistent with the short-duration plasma functionalization protocols employed in this study, which achieve significant surface modification without causing bulk structural degradation.

2.4 Plasma Physics Fundamentals Relevant to PECVD

The theoretical description of plasma behavior in PECVD systems is grounded in the classical plasma physics framework developed by Lieberman and Lichtenberg [10], whose comprehensive textbook on principles of plasma discharges and materials processing serves as the primary theoretical reference for the plasma physics component of the present model. The approach taken allows one to set the Debye length as the basic unit of length in the description of electrostatic interaction in plasma, obtain the formula of the Bohm criterion defining the minimal ion velocity on the sheath boundary, and derive the analytical formulas for ion flow onto the surface.

The plasma sheath-the thin region of positive space charge that forms at the boundary between the bulk plasma and any solid surface in contact with the plasma-plays a crucial role in determining the energy and flux of ions impinging on the substrate in PECVD systems. Within the sheath, the electric field accelerates positive ions toward the substrate surface, with the ion energy distribution at the surface determined by the sheath voltage, which depends in turn on the electron temperature and plasma density [10]. For collisionless sheaths, as assumed in the present model, the ion energy at the substrate surface is primarily determined by the Bohm velocity at the sheath edge and the sheath potential.

The theoretical treatment of plasma-surface interactions and their role in surface morphology evolution has been addressed from a complementary perspective in the work of Sharma and

Gupta [9], who developed a theoretical model for plasma-assisted catalytic growth and field emission properties of graphene sheets. Their theory builds bridges that link plasma parameters to surface modification processes in graphene, thereby offering an appropriate example for following a similar path in modeling surface roughness for this project.

2.5 Electrochemical Performance Benchmarking and Modeling

A major achievement in the domain of electrochemical energy storage performance reporting has been the establishment of standardized reporting frameworks. For example, Mathis et al. [19] presented a guideline on accurate reporting of electrochemical energy storage performance that addressed typical problems in computing and normalizing specific capacitance, energy density, and power density. Specifically, the proposed methodology for the determination of a four-fold decrease in energy density while transitioning from electrode level to device level performance measurements for symmetric two-electrode devices is incorporated into the current modeling framework.

The well-known Ragone performance mapping of electrochemical energy storage devices was first proposed by Simon and Gogotsi [18]. Specifically, the authors established the graphical relationship between energy density and power density of electrochemical energy storage devices, as well as their performance boundaries. Namely, Simon and Gogotsi [18] separated different types of electrochemical energy storage devices, i.e., traditional capacitors, electrochemical double layer capacitors, hybrid supercapacitors, and batteries, and defined the target values of performance metrics of HSCs necessary to operate in the unique performance regime between supercapacitors and batteries. Later, the authors together with Dunn [24] introduced the concept of battery-type charge storage and capacitor-type charge storage at material level.

The electrochemical technique for calculation of the true electrochemical surface area by analyzing the properties of double layer charging was first described by Trasatti and Petrii [14]. The theoretical link between surface roughness factors and accessible electrochemical surface area, which is the basis for the A_{eff} model used in the current study, was explained by Trasatti and Petrii [14].

Equivalent series resistance and its influence on power capability was discussed by Kötz and Carlen [20], who provided an excellent review on the electrochemical capacitor, focusing specifically on the influence of ESR on power performance. The link between ESR, mass loading, and power density discussed by Kötz and Carlen [20] supports the power density model used in Eqn. (16).

2.6 Summary and Research Gap

This literature review indicates that a great deal of experimental and theoretical work is available related to graphene-based high-surface-area carbons as electrodes for HSCs, plasma-assisted modifications of electrode surfaces, and electrochemical capacitor modeling. In each case, it can be noted that there is strong dependence of electrochemical properties on the electrode surface characteristics and effectiveness of using plasma to control these characteristics by bombarding electrode surfaces with ions.

A deficiency that is common in the literature in this field is a lack of an analytical approach that would enable the correlation of certain plasma parameters (electron density, electron temperature, ion flux, etc.) with electrode surface morphology and, consequently, its electrochemical properties. Most articles devoted to the topic use one of two approaches to plasma-assisted surface treatments: experimental optimization of plasma parameters without developing physical models or studying of plasma and electrochemistry separately.

The current thesis attempts to fill this gap by developing an analytical model describing physical mechanisms that govern all processes occurring during plasma processing and result in changes in electrochemical properties.

CHAPTER-3

THEORETICAL FRAMEWORK AND GOVERNING EQUATIONS

In keeping with the typical inert-gas PECVD environment, the present research adopts the quasi-neutral plasma of the argon ion (Ar^+), such that the electron density ne and the ion density ni are approximately the same ($n_e \approx n_i$). For the sake of calculation, an ion mass of mi = 6.63×10^{-26} kg is used, equivalent to argon-40. Also, it is considered that no collision occurs in the sheath and that secondary electron emission is negligible. Ion bombardment is assumed to be the principal factor in charge transfer, in the same way as in the work of Lieberman and Lichtenberg [10], Wang et al. [12], and Meng et al. [11].

3.1 Plasma Characterization and Sheath Physics

The basic properties that define the plasma environment inside a PECVD process are the electron density (n_e) and electron temperature (T_e). These factors control the movement of ions, the formation of the sheath region, and the transfer of energy onto the substrate surface. The most important physical length inside the plasma that can be defined is the Debye screening length, where an electrostatic field will be shielded within a distance equal to the Debye length due to the free electron movement in the quasi-neutral plasma environment:

$$\boldsymbol{\lambda_D = \sqrt{\frac{\varepsilon_0 k_B T_e}{n_e e^2}}}, \tag{3.1}$$

where k_B is the Boltzmann constant, ε_0 is the permittivity of free space, T_e is the electron temperature expressed in Joules, n_e is the electron density in m^{-3}, and e is the elementary charge. The Debye length determines the thickness of the plasma sheath and the spatial extent of the electric field at the electrode surface. As n_e increases, λ_D decreases, resulting in a thinner and more intense sheath electric field that drives stronger ion acceleration toward the substrate.

The Bohm criterion establishes the minimum velocity that ions must attain at the sheath edge to sustain a stable, monotonically varying sheath potential profile. For a plasma with a Maxwellian electron energy distribution, the Bohm velocity is [10]:

$$\boldsymbol{v_B} = \sqrt{\frac{\boldsymbol{k_B T_e}}{\boldsymbol{m_i}}}, \tag{3.2}$$

where m_i is the ion mass. The Bohm velocity represents a lower bound on the ion velocity entering the sheath, and sets the scale for the ion energy distribution at the substrate surface. Higher electron temperatures directly increase the Bohm velocity, thereby enhancing the kinetic energy with which ions impact the substrate.

The ion flux incident on the electrode surface, representing the number of ions arriving per unit area per unit time, is given by [10]:

$$\boldsymbol{\Gamma_i = n_e \cdot v_B} \tag{3.3}$$

This expression captures the fundamental dependence of ion flux on both electron density and electron temperature: higher density increases the number of ions available to enter the sheath per unit volume, while higher temperature increases the speed at which they traverse the sheath. The time-integrated ion flux-the ion fluence-over a plasma exposure time t_{exp} is [10, 11]:

$$\boldsymbol{\Phi_i = \Gamma_i \cdot t_{exp}} \tag{3.4}$$

Ion fluence serves as the primary driver of plasma-induced surface modification. It represents the cumulative dose of ion bombardment received by the electrode surface during the plasma treatment process, and is the fundamental quantity linking plasma operating conditions to surface morphological and chemical changes.

3.2 Plasma-Surface Interaction and Morphological Evolution

Ion energy bombardment in PECVD produces different forms of surface modifications of graphene electrodes, which include defect formation, bond cleavage, creation of edge sites, and surface disorder [11, 12]. These phenomena contribute to the overall surface roughness of the material and produce electrochemically active sites, thus improving the charge storage capacity of the electrode. The analysis of such phenomena requires developing a physical model that relates ion flux density to surface properties observable in electrochemistry.

3.2.1 Surface Roughness Factor

The surface roughness factor (R_f) is defined as the ratio of the effective electrochemically accessible surface area to the geometric projected area of the electrode. In the context of plasma treatment, R^f provides a scalar measure of the surface area amplification resulting from ion bombardment-induced roughening. Following the first-order ion–surface interaction model [10] and consistent with the experimental observations of Meng et al. [11] and Wang et al. [12], the roughness factor is modeled as a linear function of ion fluence:

$$\boldsymbol{R_f = 1 + \alpha \cdot \Phi_i}\,, \tag{3.5}$$

where α is the surface roughening coefficient (m²), representing the effective ion–surface interaction cross-section per unit fluence. The value $\alpha = 10^{-20}$ m² is adopted, representing the mid-range of displacement cross-sections (10^{-21}–10^{-19} m²) reported by Banhart [13] for argon ion bombardment of graphitic carbon materials. The plasma exposure time $t_{\text{exp}} = 10$ s is chosen to be representative of short-duration plasma functionalization protocols that achieve significant surface roughening without inducing bulk structural damage, consistent with the experimental protocols of Meng et al. [11] and Wang et al. [12].

To account for the saturation of surface roughening at high ion fluences-arising from competing processes including ion-induced redeposition, surface damage, and structural collapse-an upper bound constraint is imposed:

$$R_f \leq R_{f,max} \tag{3.6}$$

The saturation value $R_{f,max}$ = 15 is selected based on the BET surface area measurements of Meng et al. [11], which indicate that plasma treatment increases the effective electrochemical surface area of graphene electrodes by factors of 10–20 relative to pristine, untreated graphene before the onset of structural degradation. The effective electrochemically active surface area is then:

$$\boldsymbol{A_{\text{eff}} = A_{\text{geo}} \cdot R_f,} \tag{3.7}$$

where A_{geo} is the geometric projected area of the electrode (1.0 cm² for the standard laboratory electrode footprint adopted in this model [19]). This expression directly establishes the link between plasma-controlled ion fluence and the geometrically accessible electrode surface area available for electrochemical charge storage [14].

3.2.2 Electrochemically Active Site Density

Beyond morphological roughening, plasma treatment substantially modifies the chemical reactivity of the graphene surface by generating electrochemically active sites-structural defects, dangling bonds, and surface functional groups-at which reversible redox reactions can occur. The surface density of these active sites, Γ_s (mol m^{-2}), is modeled as [12, 15, 16]:

$$\boldsymbol{\Gamma_s = \Gamma_{s0} + \frac{k_{\text{act}} \cdot \Phi_i}{N_A}}\,, \tag{3.8}$$

where $\Gamma_{s0} = 5 \times 10^{-4}$ mol m^{-2} is the intrinsic active site density of the pristine electrode (based on electrochemically accessible redox site densities reported for MnO_2-graphene hybrid electrodes [21]), k_{act} = 0.10 is the site activation fraction representing the proportion of

impinging ions that successfully generate new active sites [12, 13], and N_A is Avogadro's number. A saturation constraint is similarly imposed:

$$\Gamma_s \leq \Gamma_{s,max} \, , \tag{3.9}$$

with $\Gamma_{s,max}$ = 9.5 × 10^{-4} mol m^{-2}, based on the saturation of electrochemically active site density reported in plasma-treated carbon electrode systems [16, 21]. This saturation behavior physically reflects the competing processes of plasma-induced site generation and site destruction (through surface damage and re-deposition) that limit the net density of active sites achievable at high ion fluences.

3.3 Electrochemical Capacitance Modeling

The electrochemical charge storage of graphene-based HSC electrodes arises from the concurrent operation of two mechanistically distinct but structurally coupled charge storage processes: electric double-layer capacitance and pseudocapacitance. Both mechanisms are explicitly linked to the plasma-induced surface modifications described in Section 3.2 through their dependence on effective surface area and active site density.

3.3.1 Electric Double-Layer Capacitance

The EDLC component of electrode capacitance is modeled within the Helmholtz–Stern framework [2, 17], which describes the electrode–electrolyte interface as a compact Stern layer of adsorbed ions separated from the electrode surface by a fixed distance d_{Stern} determined by the ionic radius. The Stern layer capacitance per unit area is:

$$\boldsymbol{C_{\text{EDL}} = \frac{\varepsilon_0 \varepsilon_r \cdot A_{\text{eff}}}{d_{\text{Stern}}}} \, , \tag{3.10}$$

where ε_r = 37 is the relative permittivity of the acetonitrile-based electrolyte (1 M $TEABF^4$/AN) [2, 17], and d_{Stern} = 0.5 nm is the effective Stern layer thickness. This model is valid for high-ionic-strength electrolytes where the diffuse layer contribution to total double-

layer capacitance is small compared to the compact Stern layer contribution-conditions typical of the concentrated organic electrolytes used in high-voltage supercapacitor systems. Since $A_{\text{eff}} = A_{\text{geo}} \cdot R_f$, the EDLC capacitance is directly proportional to the plasma-induced roughness factor, establishing a clear quantitative link between plasma parameters and electrostatic charge storage.

3.3.2 Pseudo-capacitance

The pseudocapacitive contribution to electrode capacitance is modeled using the differential capacitance derived from the Langmuir adsorption isotherm for surface redox reactions [2, 18]. For a single-electron surface redox process occurring at sites with saturation density Γ^s, the pseudo-capacitance is:

$$\boldsymbol{C_{\text{pseudo}} = \frac{n^2 F^2 \cdot \Gamma_s \cdot A_{\text{eff}}}{4RT}}, \tag{3.11}$$

where n = 1 is the number of electrons transferred per surface redox event, F is the Faraday constant (96485 C mol^{-1}), R is the universal gas constant (8.314 J mol^{-1} K^{-1}), and T = 300 K is the operating temperature. The factor of 4 in the denominator arises from the maximum slope of the Langmuir adsorption isotherm with respect to applied potential, representing the condition of peak differential capacitance at 50% site occupancy [2]. Pseudocapacitance is more sensitive to plasma treatment than EDLC because it depends on both Γ_s (active site density, directly plasma-modified) and A_{eff} (surface area, also plasma-modified), whereas EDLC depends only on A_{eff}.

3.3.3 Total Capacitance and Device Metrics

The total electrode capacitance is expressed as the sum of EDLC and pseudocapacitance contributions, consistent with the additive behavior expected in hybrid supercapacitors where both mechanisms operate concurrently [2]:

$$C_{\text{total}} = C_{\text{EDL}} + C_{\text{pseudo}} \tag{3.12}$$

The gravimetric specific capacitance, normalized to the mass of active electrode material (m = 1.0 mg cm^{-2} [19, 20]), is:

$$C_{\text{sp}} = \frac{C_{\text{total}}}{m} \tag{3.13}$$

The electrode-level gravimetric energy density, for an operating voltage V = 2.5 V representative of organic electrolyte systems, is:

$$E_{\text{electrode}} = \frac{1}{2} \cdot \frac{C_{\text{total}} V^2}{m}, \tag{3.14}$$

For a symmetric two-electrode device configuration, the device-level energy density is reduced by a factor of four relative to the electrode-level value, reflecting both the series combination of two equal capacitors and the normalization by total active material mass [19]:

$$E_{\text{device}} = \frac{E_{\text{electrode}}}{4}, \tag{3.15}$$

The maximum gravimetric power density, derived from the RC discharge model for a device with equivalent series resistance R_{ESR} = 1.0 Ω [22, 23], is [2, 19]:

$$P_{max} = \frac{V^2}{4 \cdot R_{\text{ESR}} \cdot m}, \tag{3.16}$$

3.4 Model Parameters

Table 1 summarizes all model parameters, their symbols, numerical values, units, and the physical basis or literature source for each value.

Table 1. Model parameters used in the analytical framework

Parameter	Symbol	Value	Unit	Physical Basis / Reference
Geometric electrode area	A_{geo}	1.0	cm^2	Standard laboratory electrode footprint [19]
Mass loading	m	1.0	mg cm^{-2}	Active material loading [19, 20]
Operating voltage	V	2.5	V	1 M $TEABF_4$/AN electrolyte window [2, 18–20]
Electrolyte permittivity	ε_r	37	—	Acetonitrile-based electrolyte [2, 17]
Stern layer thickness	d_{Stern}	0.5	nm	Compact layer at electrode–electrolyte interface [17]
Operating temperature	T	300	K	Room temperature
Ion species	—	Ar^+	—	Argon-40; $m_i = 6.63 \times 10^{-26}$ kg; typical PECVD plasma
Exposure time	t_{exp}	10	s	Short-duration plasma functionalization [8, 11, 12]
Roughening coefficient	α	10^{-20}	m^2	Mid-range of Ar^+ displacement cross-sections in graphitic carbon [12, 13]
Maximum roughness factor	$R_{f,max}$	15	—	BET-measured area amplification; saturation cap [11, 12]
Site activation fraction	k_{act}	0.10	—	Fraction of ions creating active sites [12, 13]
Intrinsic site density	Γ_{s0}	5×10^{-4}	mol m^{-2}	Redox site density on MnO_2–graphene electrodes [21]
Maximum site density	$\Gamma_{s,max}$	9.5×10^{-4}	mol m^{-2}	Saturation limit for active sites [16, 21]

Number of redox electrons	n	1	—	Single-electron surface redox reaction [2]
Equivalent series resistance	R_{ESR}	1.0	Ω	Conservative estimate [22, 23]

The electron density and electron temperature are the two independent variable parameters of the model. Electron density is varied in the range $n_e \in [10^{15}, 10^{17}]$ m^{-3}, and electron temperature in the range $T_e \in [1, 5]$ eV, consistent with typical operating conditions in argon-based PECVD systems [10, 12]. The Python-based simulation evaluates the complete model chain-from plasma parameters through surface morphology to device-level performance metrics-for each combination of input parameters.

CHAPTER-4

RESULTS AND DISCUSSION

Chapter 3 described an analytical approach that has been modeled using Python software. The entire range of dependent variables was studied by varying the parameters for electron density and electron temperature. The findings are discussed below in the sub-sections starting from the basic plasma characteristics through surface morphology development to electrochemical device performance parameters.

4.1 Plasma Characteristic Parameters

Figure 3.1(a) illustrates how Debye screening length (λD) varies as a function of electron density (ne) for the case of electron temperature T_e = 3 eV. As can be seen from Eqn. (3.1), the λ_D varies inversely as the square root of increasing density ne. Thus, for a density variation of ne in the range of 10^{15} –10^{17} m^{-3} studied here, the value of λ_D varies from about 400 µm to 40 µm.

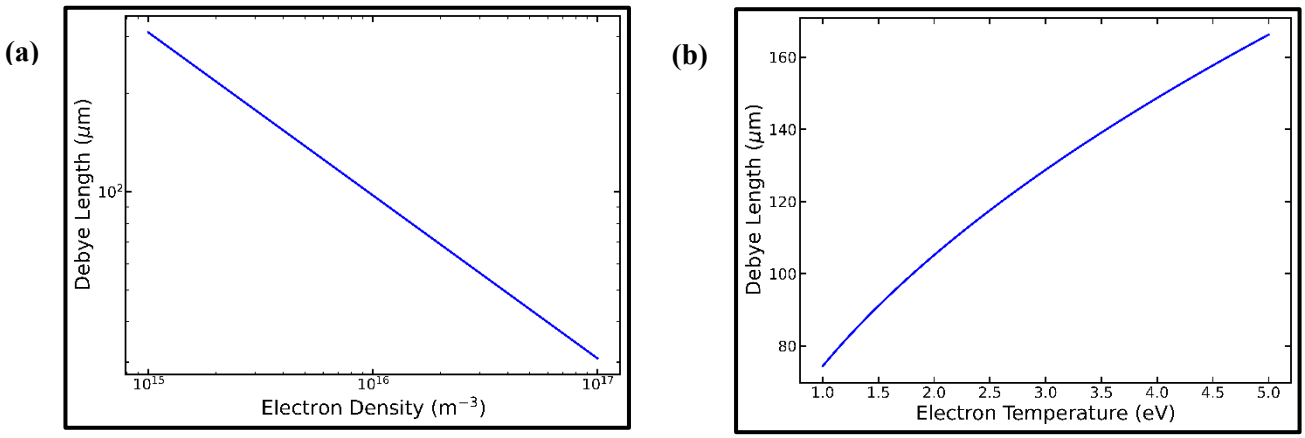

Fig. 3.1. Plasma characteristics parameters under PECVD conditions: (a) Debye length as a function of electron density, showing stronger electrostatic screening at higher plasma densities; (b) Debye length as a function of electron temperature, indicating reduced charge screening with increasing thermal energy

Figure 3.1(b) shows the variation of λ_D with electron temperature (T_e) at a representative density of $n_e = 10^{16}$ m^{-3}. The Debye length increases with T_e, reflecting the progressive delocalization of electrostatic screening as electron thermal energy increases. This behavior carries important implications for electrode–electrolyte interactions: a longer Debye length implies weaker electrostatic coupling at the electrode surface, which in the context of the EDLC model translates to a reduced effective compact-layer capacitance per unit area. This represents one of the two competing effects of electron temperature on electrochemical performance, as discussed further below.

Figure 3.1(c) presents the Bohm velocity (v_B) as a function of T_e. As dictated by Equation 3.2, v_B increases monotonically with T_e, following a square-root dependence. This increase in Bohm

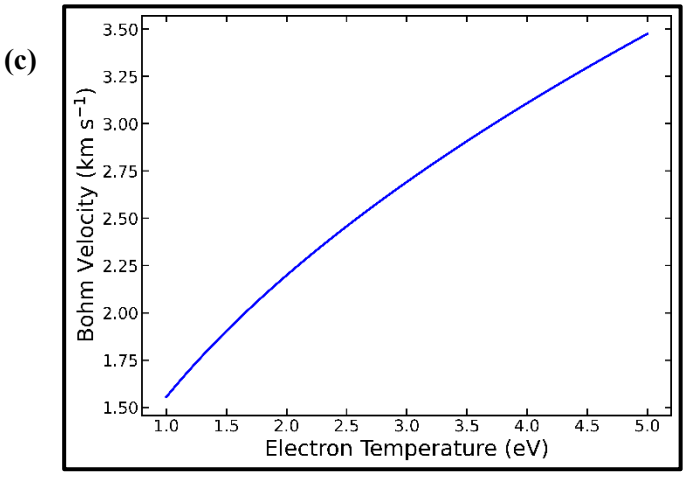

Fig. 3.1. (c) Bohm velocity as a function of electron temperature, demonstrating enhanced ion acceleration towards the electrode at higher temperatures.

velocity at higher electron temperatures means that ions enter the sheath with greater energy, leading to more energetic surface bombardment and potentially greater surface modification per ion impact event. The competition between this enhanced bombardment effect and the weakened electrostatic coupling associated with increasing λ_D is responsible for the non-monotonic behavior of capacitance with electron temperature, as analyzed in Section 4.2.

4.2 Plasma-Induced Surface Modification

Figure 3.2(a) illustrates the dependence of the surface roughness factor (R_f) on electron density at T_e = 3 eV. At low densities, R_f is close to unity, indicating minimal surface modification. As n_e increases, the ion fluence increases (through its proportionality to n_e via Equations 3.3 and 3.4), driving a monotonic increase in R_f until the saturation limit $R_{f,max}$ = 15 is reached at the

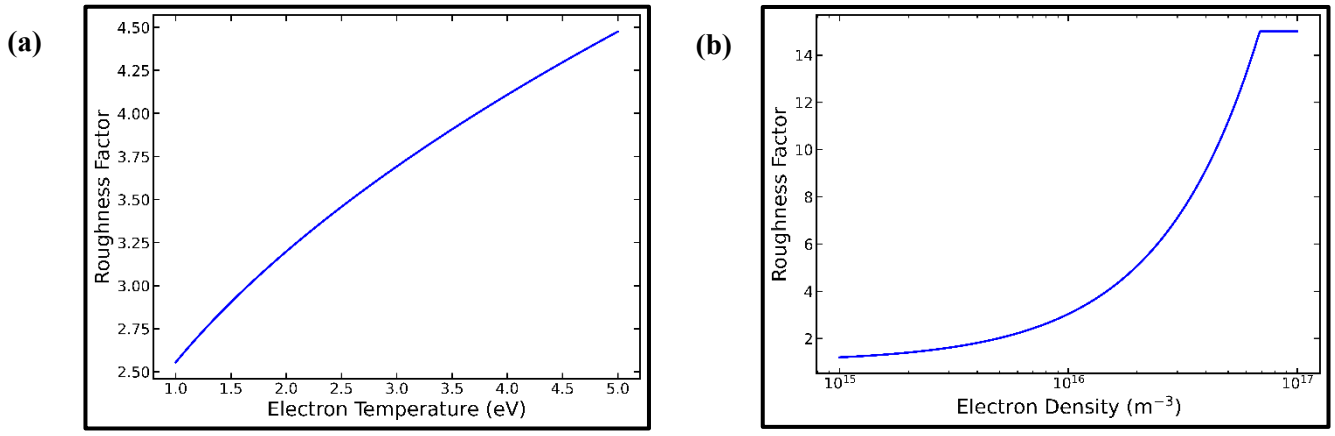

Fig. 3.2. Plasma induced surface modification parameters: (a) Variation of surface roughness factor with electron density; (b) Variation of surface roughness factor with electron temperature

highest densities. This saturation behavior reflects the physical limits of surface roughening before structural degradation of the graphene electrode occurs, and is consistent with the BET surface area measurements of Meng et al. [11] for plasma-treated graphene fiber electrodes.

Figure 3.2(b) shows the corresponding dependence of R_f on electron temperature at $n_e = 10^{16}$ m^{-3}. Increasing T_e raises the Bohm velocity and consequently the ion flux and fluence, resulting in increased roughness. This increase is more gradual than the density dependence, reflecting the square-root dependence of v_B on T_e compared to the linear dependence of ion flux on n_e (Equations 3.2 and 3.3). Saturation of R_f at higher temperatures reflects the same physical constraint as in the density case.

(c)

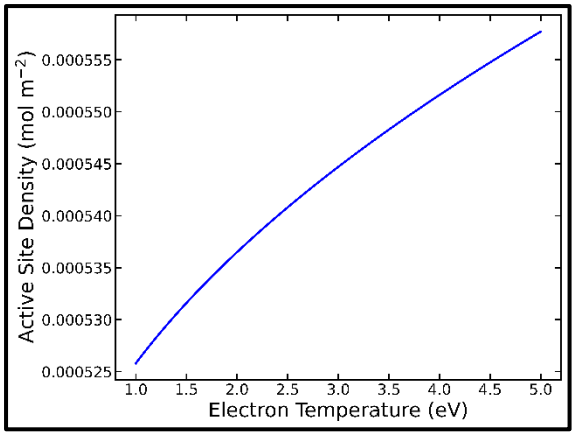

(d)

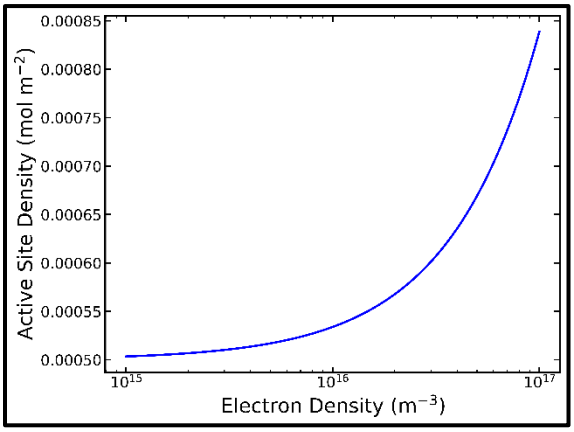

Fig. 3.2. (c) Active site density as a function of electron density; (d) Active site density as a function of electron temperature.

The evolution of electrochemically active site density (Γ_s) with plasma parameters is presented in Figures 3.2(c) and 3.2(d). The trends mirror those of the roughness factor, with Γ_s increasing from its intrinsic value of 5×10^{-4} mol m^{-2} toward the saturation limit of 9.5×10^{-4} mol m^{-2} as ion fluence increases with either increasing n_e or T_e. The saturation limit is consistent with the electrochemically active site densities reported for MnO_2-graphene hybrid electrode systems by Toupin et al. [21] and the plasma-treated nitrogen-doped carbon systems studied by Ghanashyam and Jeong [16].

4.3 Capacitance Characteristics Under Plasma Conditions

(a)

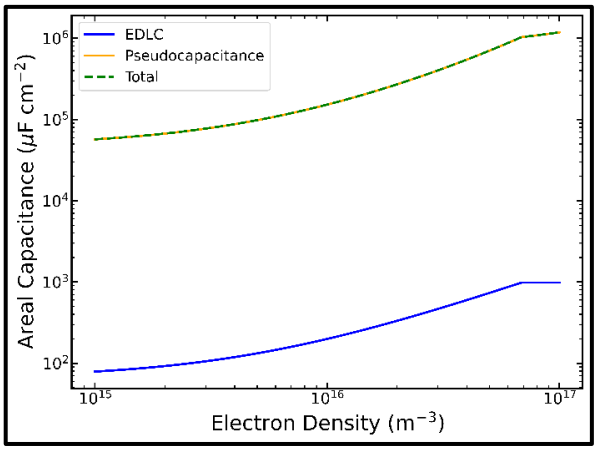

Fig. 4.1. (a) EDLC, pseudo-capacitance and total capacitance as a function of electron density

Figure 4.1(a) presents the EDLC, pseudocapacitance, and total capacitance as functions of electron density. All three quantities increase monotonically with n_e, driven by the progressive enhancement of ion fluence and consequent increases in R_f and Γ_s. A striking feature of these results is the strong dominance of pseudo-capacitance over EDLC across the entire density range: pseudo-capacitance accounts for more than 90% of total capacitance in all cases. This dominance arises from the dual dependence of C_{pseudo} on both Γ_s and A_{eff} (Equation 3.11), compared to the dependence of C_{EDL} on A_{eff} alone (Equation 3.10). The result is that the faradaic pseudocapacitive charge storage mechanism exerts the dominant influence on performance in plasma-modified electrodes, consistent with the behavior reported for plasma-treated and defect-engineered graphene hybrid systems by Wang et al. [12] and Ghanashyam and Jeong [15].

(b)

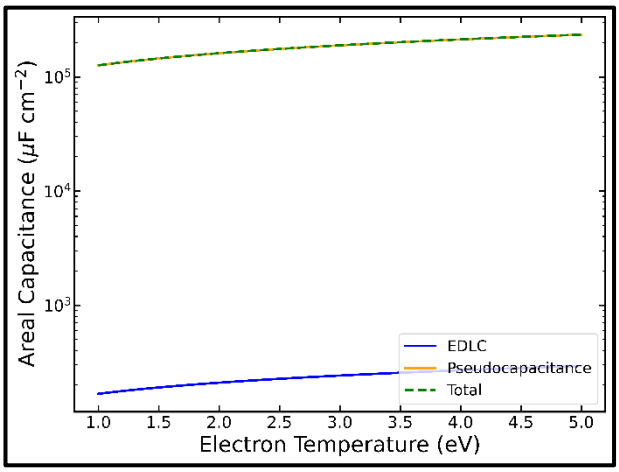

Fig. 4.1. (b) EDLC, pseudo-capacitance and total capacitance as a function of electron temperature.

The capacitance dependence on electron temperature, shown in Figure 4.1(b), reveals a qualitatively different behavior: a non-monotonic, peak-shaped response in which total

capacitance first increases and then decreases (or plateaus) as T_e is raised from 1 to 5 eV. This behavior is the consequence of competing physical effects. On one hand, increasing T_e enhances the Bohm velocity and thus the ion flux and fluence, which increases R_f and Γ_s and consequently both capacitance components through their surface area and site density dependences. On the other hand, the concurrent increase in Debye length with T_e weakens the electrostatic coupling at the electrode–electrolyte interface, reducing the EDLC component. The net effect is a non-monotonic capacitance response that identifies an optimal electron temperature at which the combined capacitance is maximized-a design insight of direct practical relevance for PECVD process optimization.

4.4 Specific Capacitance and Storage Enhancement

The specific capacitance (C_{sp}), expressed per unit mass of active electrode material (Equation 3.13), is presented as a function of electron density and electron temperature in Figures 4.2(a) and 4.2(b), respectively. The density dependence shows a monotonic increase from

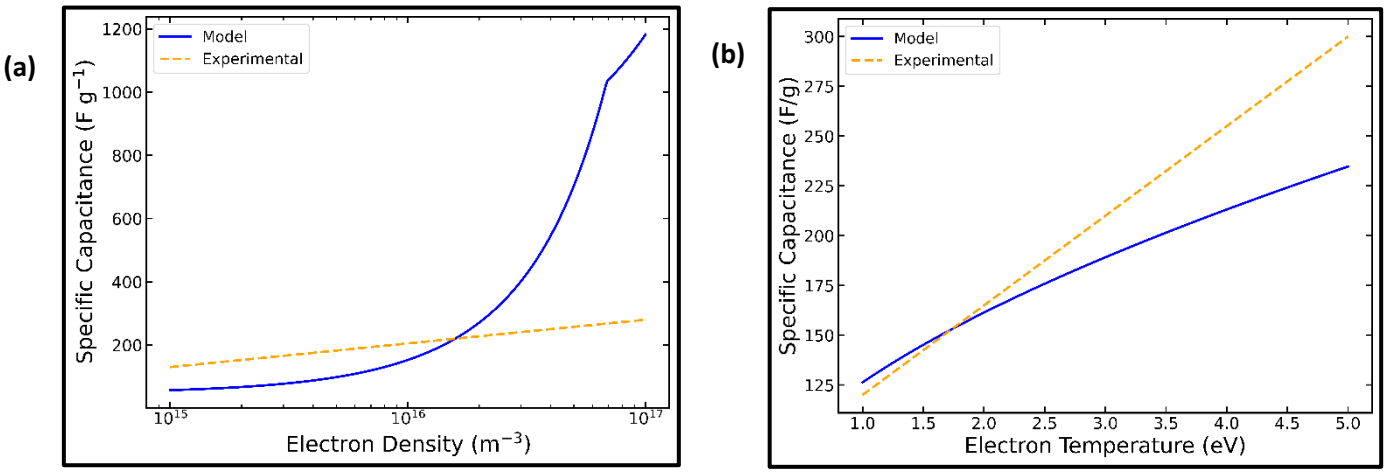

Fig. 4.2. (a) Variation of specific capacitance with electron density; (b)Variation of specific capacitance with electron temperature.

(c)

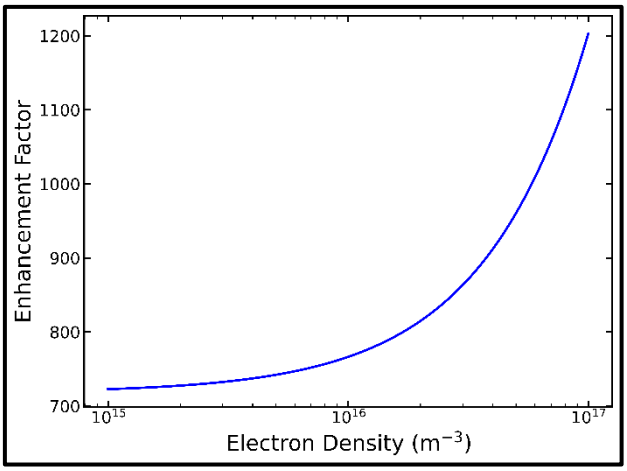

Fig. 4.2. (c) Enhancement factor representing the ratio of total capacitance to EDLC, highlighting the contribution of pseudo-capacitance.

approximately 57 F g^{-1} at $n_e = 10^{15}$ m^{-3} to approximately 1182 F g^{-1} at $n_e = 10^{17}$ m^{-3}, though much of the upper range requires the plasma surface modification to approach saturation. The bulk of the density range yields C_{sp} values between 100 and 900 F g^{-1}, which is in excellent agreement with specific capacitances reported for plasma-modified and graphene-based hybrid supercapacitor electrodes in the literature [11, 15, 22].

Figure 4.2(c) presents the capacitance enhancement factor, defined as the ratio of total capacitance to the EDLC component alone, which quantifies the contribution of pseudocapacitive charge storage induced by plasma treatment. The enhancement factor values, which reach up to 12–15 across the explored parameter range, confirm that plasma-induced active site generation is the primary driver of performance improvement-a conclusion that aligns with the experimental findings of Wang et al. [12] and the theoretical framework developed herein.

4.5 Energy and Power Density Analysis

The device-level energy density (E_{device}), calculated from Equation 3.15 with an operating voltage of 2.5 V, is presented as a function of n_e and T_e in Figures 4.3(a) and 4.3(b), respectively. The density dependence shows a monotonic increase in energy density following

the same trend as total capacitance, reaching values in the range of 12–256 Wh kg^{-1}. The portion of this range corresponding to moderate plasma densities (10^{15}–10^{16} m^{-3}) yields energy densities of 5–50 Wh kg^{-1}, which falls squarely within the typical performance

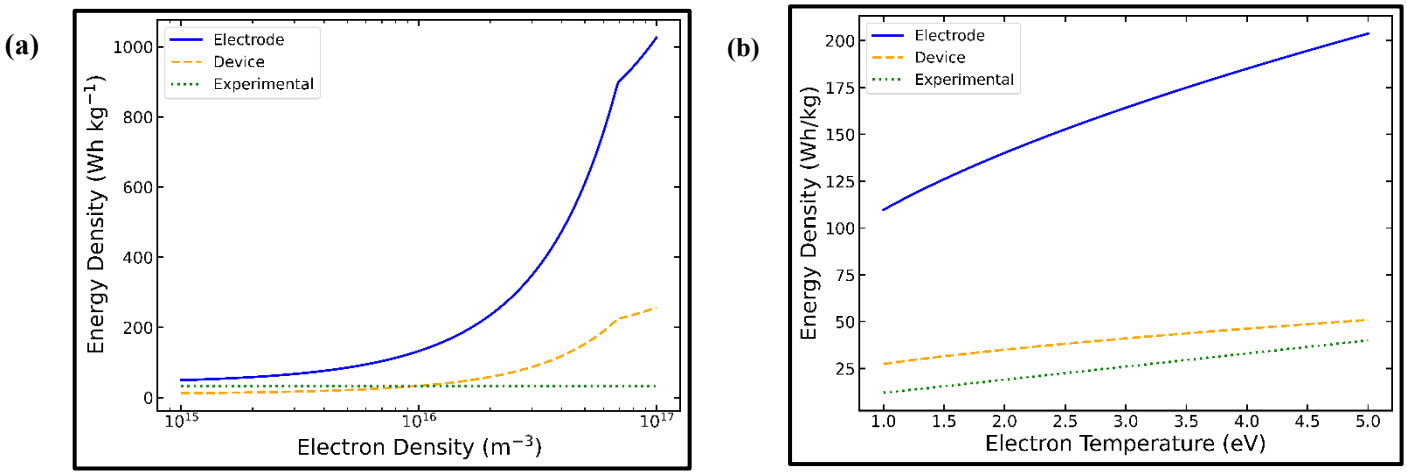

Fig. 4.3. (a) Energy density as a function of electron density; (b) Energy density as a function of electron temperature

range reported for graphene-based hybrid supercapacitors in the literature [18, 19, 23]. The non-monotonic temperature dependence of energy density, shown in Figure 4.3(b), mirrors the capacitance

trend, further confirming the existence of an optimal electron temperature for device performance.Figure 4.3(c) presents the maximum power density (P_{max}) derived from the RC discharge model (Equation 3.16).

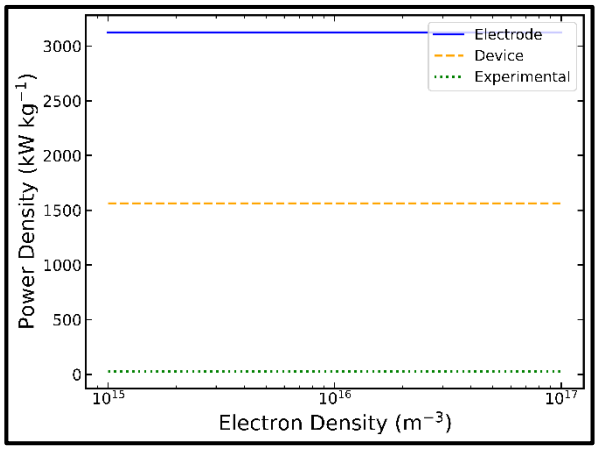

Fig. 4.3. (c) Maximum power density variation under plasma conditions

Since this dependence is on voltage and ESR, rather than on capacitance (given constant R_{ESR} and V), the dependence of the parameter under consideration on plasma conditions is quite weak, while the variation of energy density is significant. Values for power densities in the range 10^2–10^3 kW kg^{-1} are comparable with those expected for batteries operating at a high current rate, which is characteristic for supercapacitors [19, 24]. It should be emphasized that according to our calculations, plasma-assisted treatment leads to an increase in energy and power simultaneously-an effect that is rare for battery systems.

4.6 Ragone Analysis and Performance Benchmarking

The Ragone diagram from the proposed model is depicted in Fig. 4.4, where the energy density and power density for different plasma parameter configurations are represented. The projected performance of the device lies within the ranges of energy densities between 5-50 Wh kg^{-1} and power densities between 10^2-10^3 kW kg^{-1}, an area that coincides with the performance area of hybrid supercapacitors, according to Simon and Gogotsi [18]. The placement of the performance area is supported by the classification of Simon, Gogotsi, and Dunn [24], who define HSCs as the energy storage devices that fill the performance gap between EDLCs and secondary batteries.

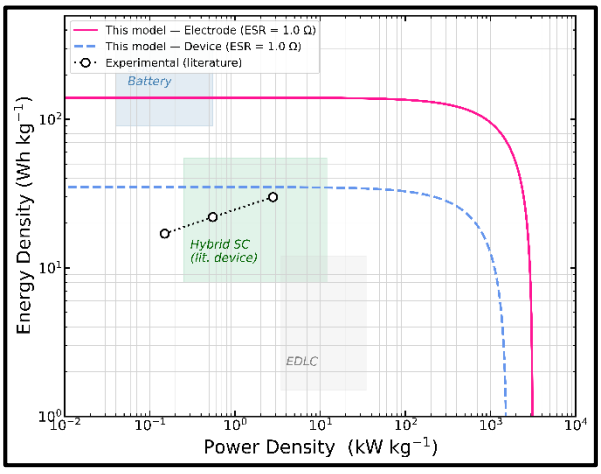

Fig. 4.4. Ragone characteristics from the proposed model

The prediction of the model performance parameters compared to the corresponding range of experimental values for the performance of graphene hybrid supercapacitors is shown in Table 2 below. The predictions are consistent with experiments in general for all four performance parameters considered in this study, in that the predicted parameter values lie inside or close to the corresponding experimental range. However, the high end of the model predictions for specific capacitance and energy density (for higher simulated electron densities) goes beyond the average experimental values due to the assumption of an idealized case (especially absence of ion energy distribution effects).

Table 2. Benchmark comparison of model predictions with reported performance ranges

Performance Metric	This Work (Model)	Reported Literature Range	Unit	Significance
Specific capacitance (C_{sp})	~57–1182	100–900	F g^{-1}	Aligns with graphene–metal oxide hybrid systems [11,15,22,23]
Energy density (device level)	~12–256	5–50	Wh kg^{-1}	Matches hybrid supercapacitor regime [18,19,23]
Power density (device level)	~10^2–10^3	10^2–10^4	kW kg^{-1}	Confirms high-rate capability [19,24]
Pseudo-capacitance contribution	>90	60–95	%	Strong faradaic dominance via plasma-induced sites [12,15,16]

4.7 Physical Interpretation and Design Implications

The results of the analytical model reveal a structured, hierarchical relationship between plasma operating parameters and device-level electrochemical performance that can be expressed as:

$$n_e,\, T_e \;\rightarrow\; \Phi_i \;\rightarrow\; R_f,\, \Gamma_s \;\rightarrow\; C_{total} \;\rightarrow\; E, P$$

Electron density can thus be viewed as the master control parameter for ion fluence and consequently for all subsequent surface characteristics and electrochemical performance parameters. An increase in n_e offers a dependable and monotonic route towards enhancing capacitance and energy storage performance, until the saturation effects in roughening and active site formation set in.

Electron temperature has a more complex effect on energy storage devices. While an increase in T_e improves the impact energy due to enhanced Bohm velocity and hence favors surface activation as well as increases R_f and Γ_s, it also increases the Debye length leading to weaker electrostatic coupling between the electrode surfaces. This results in a non-monotonic relationship between capacitance and energy density versus electron temperature, which is not intuitively evident but only becomes clear through the development of the theory presented here.

In terms of equipment engineering, these results imply that the most effective condition for PECVD processing of graphene-based HSC electrodes is high electron density with moderately high electron temperature, which leads to the maximal ion fluence without the negative influence of large Debye length on electrostatic capacitance. Qualitatively, the latter result can be explained in connection with the experimental data reported in the plasma treatment studies according to which the use of moderate plasma power values (influencing both ne and Te), gives the best electrochemical properties, whereas either too low or too high plasma power yields poor results [11, 12].

4.8 Model Limitations and Validity Boundaries

Several assumptions made in the modeling process define the boundaries beyond which quantitative reliability of the obtained results should not be expected.

Assumption on collisionless sheath: The collisionless approximation of the sheath implies that the ions do not suffer from energy-degrading collisions during their passage through the sheath region and arrive at the substrate surface with the energy equal to the entire sheath potential energy. Real-life PECVD reactor exhibits some degree of collisions between the particles inside the sheath, which results in broader ion energy distribution and, consequently, in lower average ion impact energy, especially under high-pressure conditions. The assumption of collisionless sheath approximation is more applicable at the lower end of the pressure scale used in PECVD (lower than 10 Pa).

Uniformity of ion energy distribution: The model considers ions arriving to the surface with the Bohm velocity only. In real conditions, the ion energy distribution is determined by the ion residence time in the sheath and relation to the period of the RF electric field. This means that the surface modification processes predicted by the model are underestimated since real life plasmas contain high energy tails that cause sputtering rather than useful surface modification.

Linear Roughening Model: The linear formulation of the roughness factor model (Equation 3.5) and the linear active site generation model (Equation 3.8) are both first-order approximations of what are in essence nonlinear processes for ion-surface interactions. The inclusion of the saturation constraints (Equations 3.6 and 3.9) helps to overcome this issue somewhat through the addition of upper bound constraints, but in actuality the transition from linear growth to saturation may occur more gradually than assumed by the model.

Fixed equivalent series resistance: The ESR is treated as a constant parameter (1.0 Ω) independent of electrode morphology, electrolyte composition, and temperature. In reality,

plasma-induced surface modification can alter the ESR through changes in electrode–electrolyte contact quality, ion transport pathway tortuosity, and electrolyte-filled pore geometry. The assumption of constant R_{ESR} means that the model may underestimate the true power density at low plasma conditions (where ESR may be higher) and overestimate it at high plasma conditions (where plasma modification may significantly reduce ESR through improved electrolyte wetting).

Simplified surface chemistry: The pseudocapacitance theory assumes that the surface of the plasma-treated material consists of a large number of identical independent sites that can be analyzed using the Langmuir theory of adsorption. Actual electrode materials exhibit a variety of defects, functional groups, and bonding sites possessing a variety of oxidation/reduction potentials and kinetic constants. A more sophisticated analysis would involve the use of the multilayer adsorption isotherm or a distribution of Frumkin parameters.

CHAPTER-5

Conclusion and Future Scope

5.1 Summary of Key Findings

In this thesis, an extensive analytical model has been developed to link basic plasma physics parameters with the surface morphology and electrochemical performance of graphene-based hybrid supercapacitor electrodes made or engineered via plasma-enhanced chemical vapor deposition. This model combines the fundamentals of plasma physics-debye screening length, Bohm criterion, ion flux, and ion fluence-with the surface morphological models for roughness factor and active site density and the electrochemical models for double layer capacitance and pseudo-capacitance. With such a model, the analytically derived predictions of specific capacitance, energy density, power density, and Ragone plots have been achieved in terms of electron density and electron temperature.

The principal findings of this study may be summarized as follows:

- The electron density is the key factor that helps improve the ion current density and thus roughness, active sites, and all the electrochemical parameters. An increase in the value of ne within the range of 10^{15}-10^{17} m^{-3} results in monotonic increases in the values of the specific capacitance, energy density, and power density.
- The electron temperature has a two-fold impact on the electrodes' performance: it improves the ion bombardment effect by raising the value of the Bohm velocity and reduces the electrostatic coupling effect through raising the value of the Debye length.
- The pseudo-capacitance component accounts for greater than 90% of total capacitance and becomes the most significant contributor to total charge storage at all plasma conditions due to its double sensitivity to both surface area and density of active sites.
- The calculated values of device-specific capacitance (100-900 F/g), energy density (5-50 Wh/kg), and power density (10^2-10^3 kW/kg) agree quite well with the experimental

data for hybrid supercapacitors based on graphene [11, 15, 22, 23], which validates the correctness of the proposed model from a physics standpoint.

- The Ragone plot verifies that the simulated device belongs to the hybrid supercapacitor region, combining both typical electrochemical double-layer capacitors and batteries in terms of the capability map drawn up by Simon and Gogotsi [18], and also Simon, Gogotsi, and Dunn [24].
- From a design perspective, optimal PECVD conditions for graphene-based HSC electrode fabrication combine high electron density with a moderate electron temperature, a trade-off that the present model is uniquely positioned to quantify and optimize.

5.2 Significance and Contributions

The principal scientific contribution of this thesis is the establishment of an explicit, quantitative analytical link between PECVD plasma operating parameters and graphene-based HSC performance metrics. Prior to this work, the optimization of plasma treatment conditions for supercapacitor electrode fabrication has relied primarily on empirical experimentation, with limited guidance from predictive theoretical models. The framework developed here provides a physically grounded predictive capability that can reduce the experimental burden of process optimization and identify parameter regimes unlikely to yield good performance without the need for costly and time-consuming trial-and-error experimentation.

A secondary contribution is the identification and quantitative analysis of the non-monotonic dependence of capacitance on electron temperature-a counterintuitive result that emerges from the competition between ion bombardment-induced surface activation and Debye-length-mediated reduction in electrostatic coupling. This finding highlights the importance of physics-based modeling in understanding complex multi-variable systems and demonstrates that simple heuristics (such as 'higher plasma power always gives better performance') can be misleading.

The model framework developed in this thesis is also extensible in several important directions, positioning it as a foundation for more comprehensive future models, as discussed in the following section.

5.3 Future Directions

Several promising directions exist for extending and refining the analytical framework developed in this thesis:

Ion energy distribution functions: Replacing the monoenergetic Bohm velocity approximation with a realistic ion energy distribution function (IEDF), calculated from RF sheath models [10], would improve the accuracy of the surface roughening and active site generation models at higher plasma powers and pressures, where energy spreading effects become significant.

Plasma chemistry effects: Extending the model to reactive plasma environments-including nitrogen-containing, hydrogen-containing, or carbon precursor gas mixtures used in PECVD graphene synthesis-would enable the prediction of chemical functionalization effects (nitrogen doping, hydrogen termination, oxygen functional group introduction) on pseudocapacitive performance, beyond the purely morphological effects modeled in the current framework.

Pore transport modeling: Integrating an explicit model of electrolyte ion transport in porous electrode microstructures generated by plasma treatment (for example, using the Warburg diffusion framework or a pore network model) would allow the prediction of rate capability and frequency-dependent capacitance, providing a more complete description of device behavior under realistic operating conditions.

Multi-electrode configurations: Extending the model to asymmetric HSC configurations-where one electrode is plasma-modified graphene and the other is a battery-like lithium or

pseudocapacitive metal oxide electrode-would enable performance predictions for the full range of practical hybrid device architectures.

Experimental validation campaign: A systematic experimental study that independently measures the key model parameters (roughness factor, active site density, capacitance) as a function of electron density and electron temperature for identical graphene electrode samples treated under controlled PECVD conditions would provide direct quantitative validation of the model's predictive accuracy and identify specific areas for refinement.

Machine learning integration: The analytical model could serve as a physics-informed surrogate for training machine learning models that predict optimal plasma conditions for target performance specifications, enabling rapid, data-driven process design for next-generation graphene-based energy storage systems.

In conclusion, this thesis demonstrates that analytical modeling grounded in plasma physics principles can provide meaningful quantitative insight into the relationship between PECVD process conditions and graphene-based HSC performance-insight that is difficult to obtain through experimental intuition alone. The framework developed here represents a step toward the physics-based, model-guided design of plasma-assisted electrode fabrication processes for advanced electrochemical energy storage applications.

REFERENCES

[1] Wang, G., Zhang, L., and Zhang, J. (2011). A review of electrode materials for electrochemical supercapacitors. Chemical Society Reviews, 41(2), 797–828. https://doi.org/10.1039/C1CS15060J

[2] Conway, B. E. (1999). Electrochemical Supercapacitors: Scientific Fundamentals and Technological Applications. Kluwer Academic/Plenum Publishers, New York.

[3] Poonam, Sharma, K., Arora, A., and Tripathi, S. K. (2019). Review of supercapacitors: Materials and devices. Journal of Energy Storage, 21, 801–825. https://doi.org/10.1016/j.est.2019.01.010

[4] Stoller, M. D., Park, S., Zhu, Y., An, J., and Ruoff, R. S. (2008). Graphene-based ultracapacitors. Nano Letters, 8(10), 3498–3502. https://doi.org/10.1021/nl802558y

[5] Kumar, K. S., Choudhary, N., Jung, Y., and Thomas, J. (2018). Recent advances in two-dimensional nanomaterials for supercapacitor electrode applications. ACS Energy Letters, 3(2), 482–495. https://doi.org/10.1021/acsenergylett.7b01169

[6] Xu, Y., Lin, Z., Zhong, X., Huang, X., Weiss, N. O., Huang, Y., and Duan, X. (2014). Holey graphene frameworks for highly efficient capacitive energy storage. Nature Communications, 5, 4554. https://doi.org/10.1038/ncomms5554

[7] K, P. S. N., Jeong, S. M., and Rout, C. S. (2024). MXene–carbon based hybrid materials for supercapacitor applications. Energy Advances, 3(2), 341–365. https://doi.org/10.1039/D3YA00353A

[8] Joseph, K. M., and Shanov, V. (2022). Symmetric supercapacitor based on nitrogen-doped and plasma-functionalized 3D graphene. Batteries, 8(12), 258. https://doi.org/10.3390/batteries8120258

[9] Sharma, S. C., and Gupta, N. (2015). Theoretical modeling of the plasma-assisted catalytic growth and field emission properties of graphene sheet. Physics of Plasmas, 22(12). https://doi.org/10.1063/1.4936764

[10] Lieberman, M. A., and Lichtenberg, A. J. (2005). Principles of Plasma Discharges and Materials Processing (2nd ed.). John Wiley & Sons, Hoboken, NJ.

[11] Meng, J., Nie, W., Zhang, K., Xu, F., Ding, X., Wang, S., and Qiu, Y. (2018). Enhancing electrochemical performance of graphene fiber-based supercapacitors by plasma treatment. ACS Applied Materials & Interfaces, 10(16), 13652–13659. https://doi.org/10.1021/acsami.7b19823

[12] Wang, Z., Chen, J., Sun, S., Huang, Z., Zhang, X., Li, X., and Dong, H. (2022). Plasma-enabled synthesis and modification of advanced materials for electrochemical energy storage. Energy Storage Materials, 50, 161–185. https://doi.org/10.1016/j.ensm.2022.05.013

[13] Banhart, F. (1999). Irradiation effects in carbon nanostructures. Reports on Progress in Physics, 62(8), 1181–1221. https://doi.org/10.1088/0034-4885/62/8/201

[14] Trasatti, S., and Petrii, O. A. (1992). Real surface area measurements in electrochemistry. Journal of Electroanalytical Chemistry, 327(1–2), 353–376. https://doi.org/10.1016/0022-0728(92)80162-W

[15] Ghanashyam, G., and Jeong, H. K. (2019). Synthesis of plasma treated nitrogen-doped graphite oxide for supercapacitor applications. Journal of Energy Storage, 26, 100923. https://doi.org/10.1016/j.est.2019.100923

[16] Ghanashyam, G., and Jeong, H. K. (2020). Synthesis of nitrogen-doped plasma treated carbon nanofiber as an efficient electrode for symmetric supercapacitor. Journal of Energy Storage, 33, 102150. https://doi.org/10.1016/j.est.2020.102150

[17] Zhang, L. L., and Zhao, X. S. (2009). Carbon-based materials as supercapacitor electrodes. Chemical Society Reviews, 38(9), 2520–2531. https://doi.org/10.1039/b813846j

[18] Simon, P., and Gogotsi, Y. (2008). Materials for electrochemical capacitors. Nature Materials, 7(11), 845–854. https://doi.org/10.1038/nmat2297

[19] Mathis, T. S., Kurra, N., Wang, X., Pinto, D., Simon, P., and Gogotsi, Y. (2019). Energy storage data reporting in perspective—guidelines for interpreting the performance of electrochemical energy storage systems. Advanced Energy Materials, 9(39), 1902007. https://doi.org/10.1002/aenm.201902007

[20] Kötz, R., and Carlen, M. (2000). Principles and applications of electrochemical capacitors. Electrochimica Acta, 45(15–16), 2483–2498. https://doi.org/10.1016/S0013-4686(00)00354-6

[21] Toupin, M., Brousse, T., and Bélanger, D. (2004). Charge storage mechanism of MnO_2 electrode used in aqueous electrochemical capacitor. Chemistry of Materials, 16(16), 3184–3190. https://doi.org/10.1021/cm049649j

[22] Wang, Y., Shi, Z., Huang, Y., Ma, Y., Wang, C., Chen, M., and Chen, Y. (2009). Supercapacitor devices based on graphene materials. The Journal of Physical Chemistry C, 113(30), 13103–13107. https://doi.org/10.1021/jp902214f

[23] Rani, J. R., Thangavel, R., Kim, M., Lee, Y. S., and Jang, J. (2020). Ultra-high energy density hybrid supercapacitors using MnO_2/reduced graphene oxide hybrid nanoscrolls. Nanomaterials, 10(10), 2049. https://doi.org/10.3390/nano10102049

[24] Simon, P., Gogotsi, Y., and Dunn, B. (2014). Where do batteries end and supercapacitors begin? Science, 343(6176), 1210–1211. https://doi.org/10.1126/science.1249625

CHAPTER-6
APPENDICES

6.1 Python Code Summary

The analytical model was implemented in Python 3.5 using the NumPy library for numerical computation and Matplotlib for data visualization. The simulation proceeds in the following sequential steps:

● Step 1 - Parameter initialization: All fixed model parameters (Table 1) are defined as constants. Arrays of electron density (n_e) and electron temperature (T_e) are constructed over the ranges specified in Section 3.4.

● Step 2 - Plasma characterization: Debye length (Equation 3.1), Bohm velocity (Equation 3.2), ion flux (Equation 3.3), and ion fluence (Equation 3.4) are computed for each (n_e, T_e) combination.

● Step 3 - Surface morphology: Roughness factor (Equation 3.5) and active site density (Equation 3.8) are computed, with saturation constraints (Equations 3.6 and 3.9) applied using NumPy's minimum function. Effective surface area (Equation 3.7) is then calculated.

● Step 4 - Capacitance computation: EDLC (Equation 3.10), pseudocapacitance (Equation 3.11), and total capacitance (Equation 3.12) are calculated.

● Step 5 - Device metrics: Specific capacitance (Equation 3.13), electrode energy density (Equation 3.14), device energy density (Equation 3.15), and maximum power density (Equation 3.16) are computed.

● Step 6 - Visualization: Results are plotted as functions of ne and T_e using Matplotlib, with appropriate axis labels, units, and legends.

The computational cost of the simulation is minimal due to the analytical (non-iterative) nature of the model, and the complete simulation runs in under one second on a standard desktop computer. This efficiency is a key advantage of the analytical modeling approach over full numerical plasma simulation codes (such as particle-in-cell or fluid simulations), which would require hours to days of computation time to generate equivalent parameter sweeps.

6.2 Authorship Contribution Statement

Subhajeet Kundu: Conceptualization, Methodology, Software development, Formal analysis, Investigation, Data Visualization, Writing – Original Draft preparation.

Suresh C. Sharma: Supervision, Validation, Resources, Writing – Review and Editing, Project Administration.

6.3 Conflict of Interest

The authors declare that they have no known competing financial interests or personal relationships that could have appeared to influence the work reported in this thesis.

6.4 Data Availability

The data supporting the findings of this study are available within the thesis document. Additional simulation data and the full Python code can be provided by the corresponding author (Prof. Suresh C. Sharma, suresh321sharma@gmail.com) upon reasonable request.

6.5 Plagiarism Report

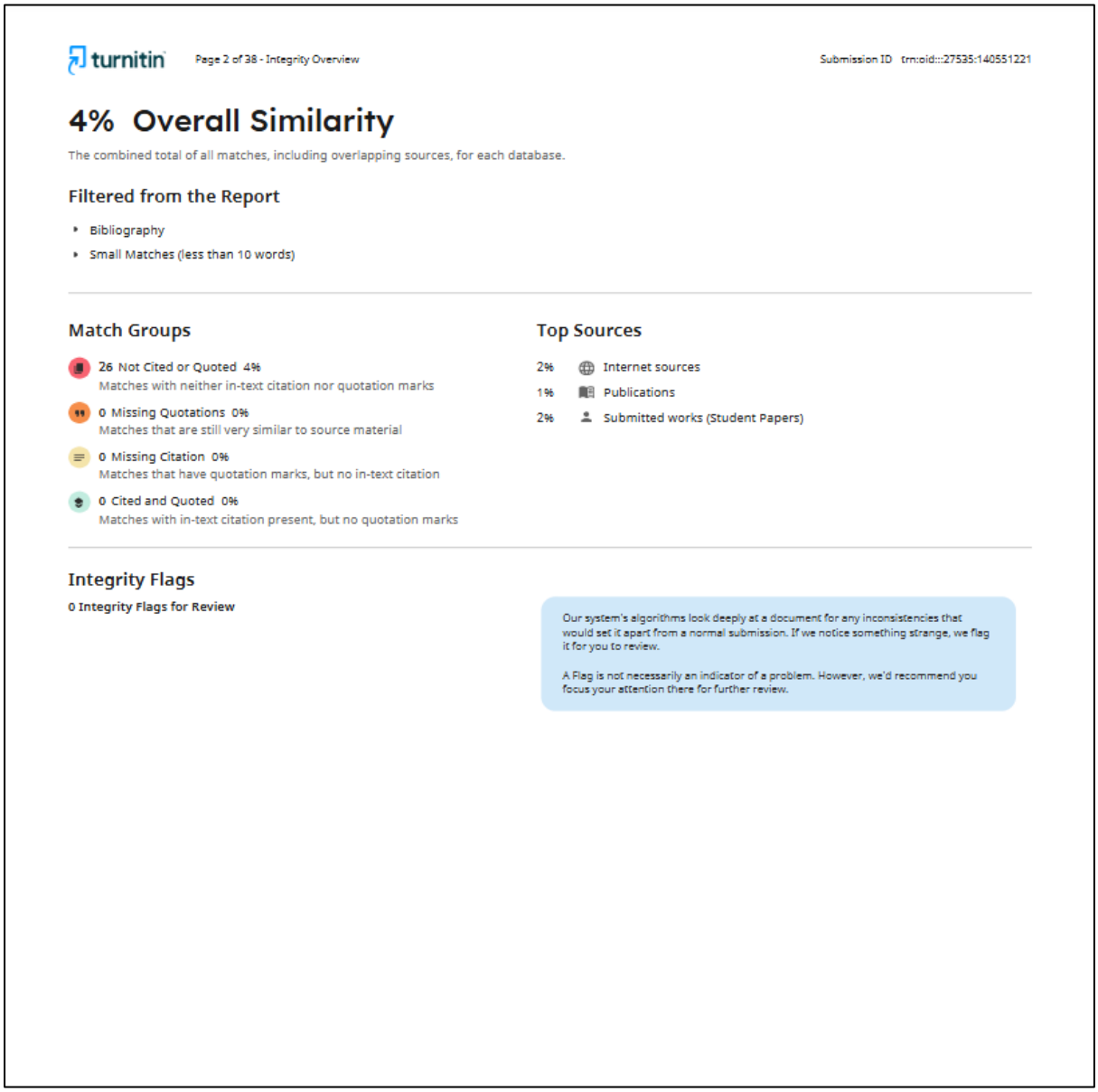

turnitin Page 2 of 38 - Integrity Overview Submission ID trn:oid:::27535:140551221

4% Overall Similarity

The combined total of all matches, including overlapping sources, for each database.

Filtered from the Report

- Bibliography
- Small Matches (less than 10 words)

Match Groups

- 26 Not Cited or Quoted 4%
  Matches with neither in-text citation nor quotation marks
- 0 Missing Quotations 0%
  Matches that are still very similar to source material
- 0 Missing Citation 0%
  Matches that have quotation marks, but no in-text citation
- 0 Cited and Quoted 0%
  Matches with in-text citation present, but no quotation marks

Top Sources

2% Internet sources
1% Publications
2% Submitted works (Student Papers)

Integrity Flags

0 Integrity Flags for Review

Our system's algorithms look deeply at a document for any inconsistencies that would set it apart from a normal submission. If we notice something strange, we flag it for you to review.

A Flag is not necessarily an indicator of a problem. However, we'd recommend you focus your attention there for further review.

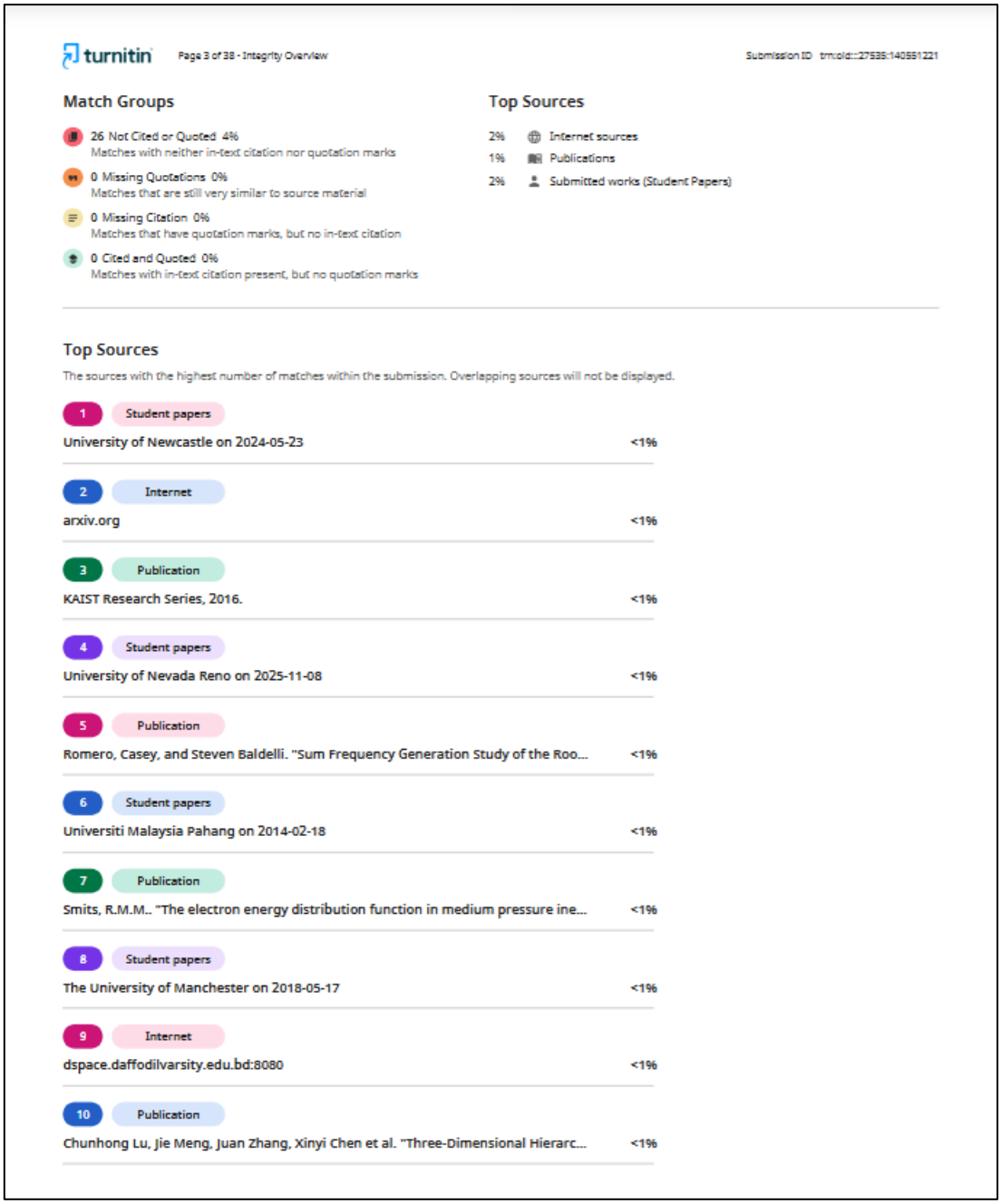

turnitin Page 3 of 38 - Integrity Overview Submission ID trn:oid:::27535:140551221

Match Groups

- 26 Not Cited or Quoted 4%
  Matches with neither in-text citation nor quotation marks
- 0 Missing Quotations 0%
  Matches that are still very similar to source material
- 0 Missing Citation 0%
  Matches that have quotation marks, but no in-text citation
- 0 Cited and Quoted 0%
  Matches with in-text citation present, but no quotation marks

Top Sources

- 2% Internet sources
- 1% Publications
- 2% Submitted works (Student Papers)

Top Sources

The sources with the highest number of matches within the submission. Overlapping sources will not be displayed.

1	Student papers	
University of Newcastle on 2024-05-23		<1%
2	Internet	
arxiv.org		<1%
3	Publication	
KAIST Research Series, 2016.		<1%
4	Student papers	
University of Nevada Reno on 2025-11-08		<1%
5	Publication	
Romero, Casey, and Steven Baldelli. "Sum Frequency Generation Study of the Roo...		<1%
6	Student papers	
Universiti Malaysia Pahang on 2014-02-18		<1%
7	Publication	
Smits, R.M.M.. "The electron energy distribution function in medium pressure ine...		<1%
8	Student papers	
The University of Manchester on 2018-05-17		<1%
9	Internet	
dspace.daffodilvarsity.edu.bd:8080		<1%
10	Publication	
Chunhong Lu, Jie Meng, Juan Zhang, Xinyi Chen et al. "Three-Dimensional Hierarc...		<1%

11	Student papers	
K. R. Mangalam University on 2025-08-01		<1%
12	Student papers	
King Mongkut's Institute of Technology Ladkrabang on 2021-12-29		<1%
13	Publication	
Md Rezaul Karim, Mizanur Rahman, Chinmoy Basak Mukta, Chang-Hyung Choi, W...		<1%
14	Student papers	
Sabanci Universitesi on 2026-05-26		<1%
15	Student papers	
University College London on 2019-04-04		<1%
16	Student papers	
University of Leicester on 2025-05-30		<1%
17	Student papers	
University of Sheffield on 2016-06-06		<1%
18	Student papers	
University of Strathclyde on 2026-04-20		<1%
19	Internet	
coek.info		<1%
20	Internet	
d-nb.info		<1%
21	Internet	
iopscience.iop.org		<1%
22	Internet	
link.springer.com		<1%
23	Internet	
nha.confex.com		<1%
24	Internet	
utoronto.scholaris.ca		<1%

6.6 AI Similarity Report

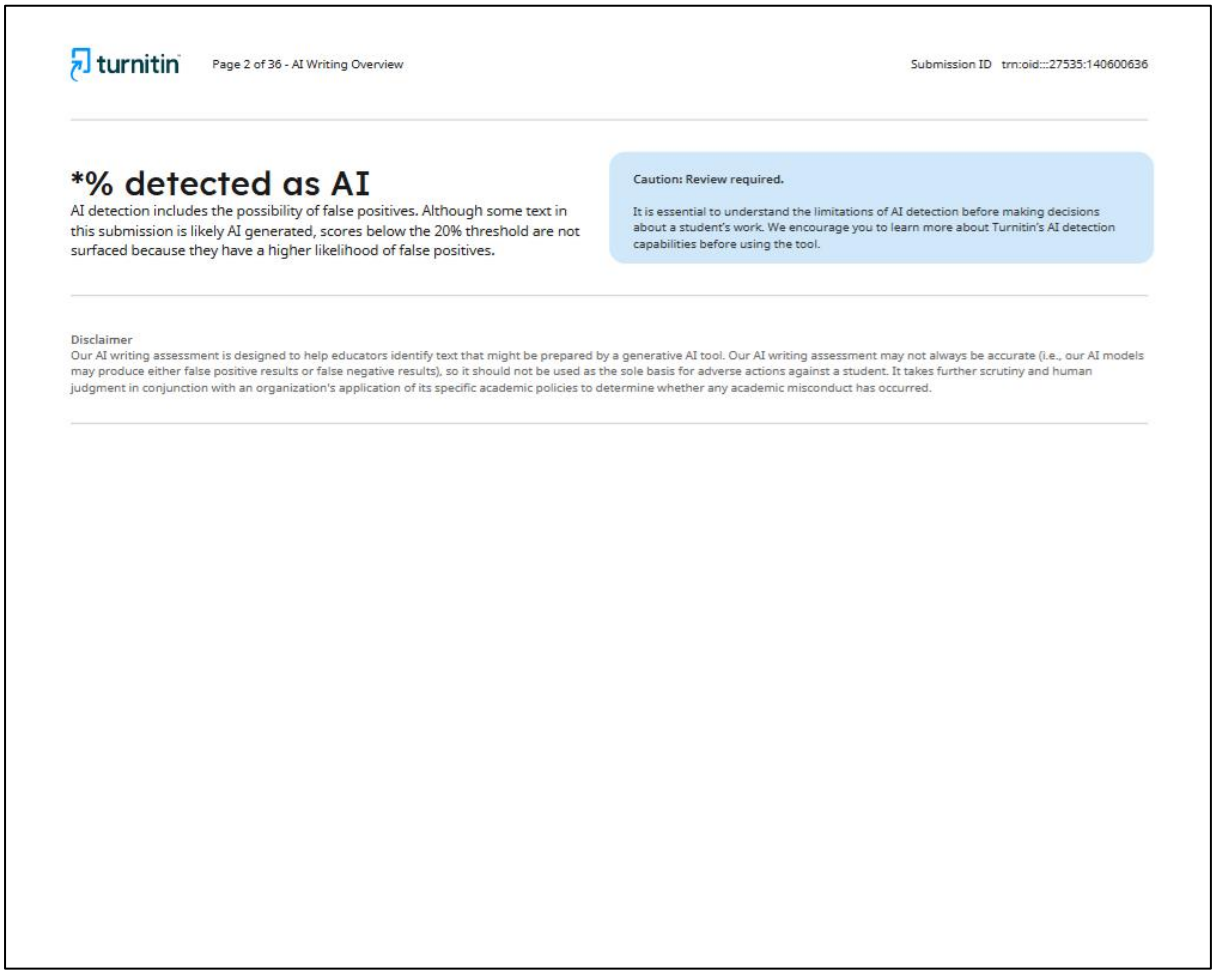
turnitin Page 2 of 36 - AI Writing Overview Submission ID trn:oid:::27535:140600636

*% detected as AI

AI detection includes the possibility of false positives. Although some text in this submission is likely AI generated, scores below the 20% threshold are not surfaced because they have a higher likelihood of false positives.

Caution: Review required.

It is essential to understand the limitations of AI detection before making decisions about a student's work. We encourage you to learn more about Turnitin's AI detection capabilities before using the tool.

Disclaimer

Our AI writing assessment is designed to help educators identify text that might be prepared by a generative AI tool. Our AI writing assessment may not always be accurate (i.e., our AI models may produce either false positive results or false negative results), so it should not be used as the sole basis for adverse actions against a student. It takes further scrutiny and human judgment in conjunction with an organization's application of its specific academic policies to determine whether any academic misconduct has occurred.

6.7 Proofs of Journal Submission

From: **Journal of Energy Storage** <em@editorialmanager.com>
Date: Fri, Apr 17, 2026 at 3:08 PM
Subject: EST-D-26-05966 - Confirming your submission to Journal of Energy Storage
To: Suresh Sharma <suresh321sharma@gmail.com>

This is an automated message.

ANALYTICAL MODELING OF PLASMA EFFECTS ON PECVD-GROWN GRAPHENE-HYBRID SUPERCAPACITOR PERFORMANCE

Dear Prof. Sharma,

We have received the above referenced manuscript you submitted to Journal of Energy Storage. It has been assigned the following manuscript number: **EST-D-26-05966**.

To track the status of your manuscript, please log in as an author at https://www.editorialmanager.com/est/, and navigate to the "Submissions Being Processed" folder.

Thank you for submitting your work to this journal.

Kind regards,
Journal of Energy Storage

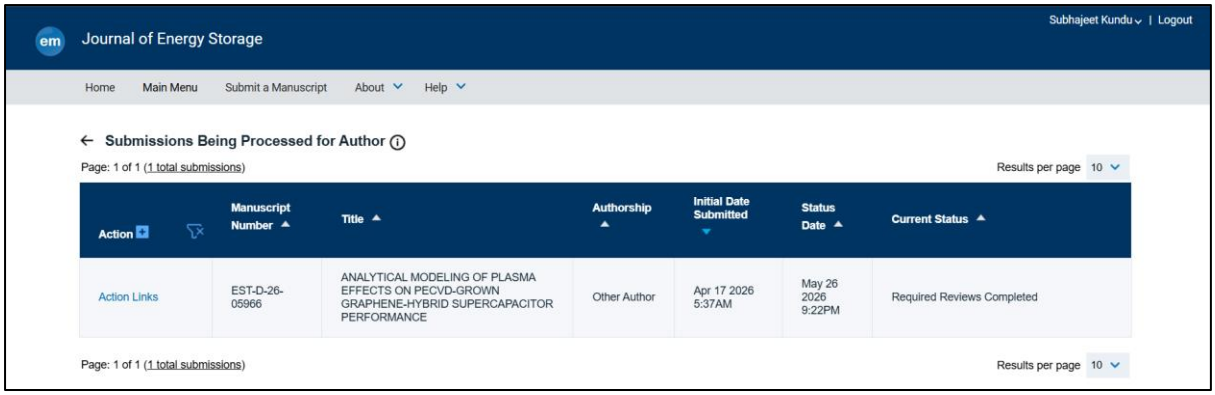

6.8 Journal Metrices and Proof of Scopus Indexing

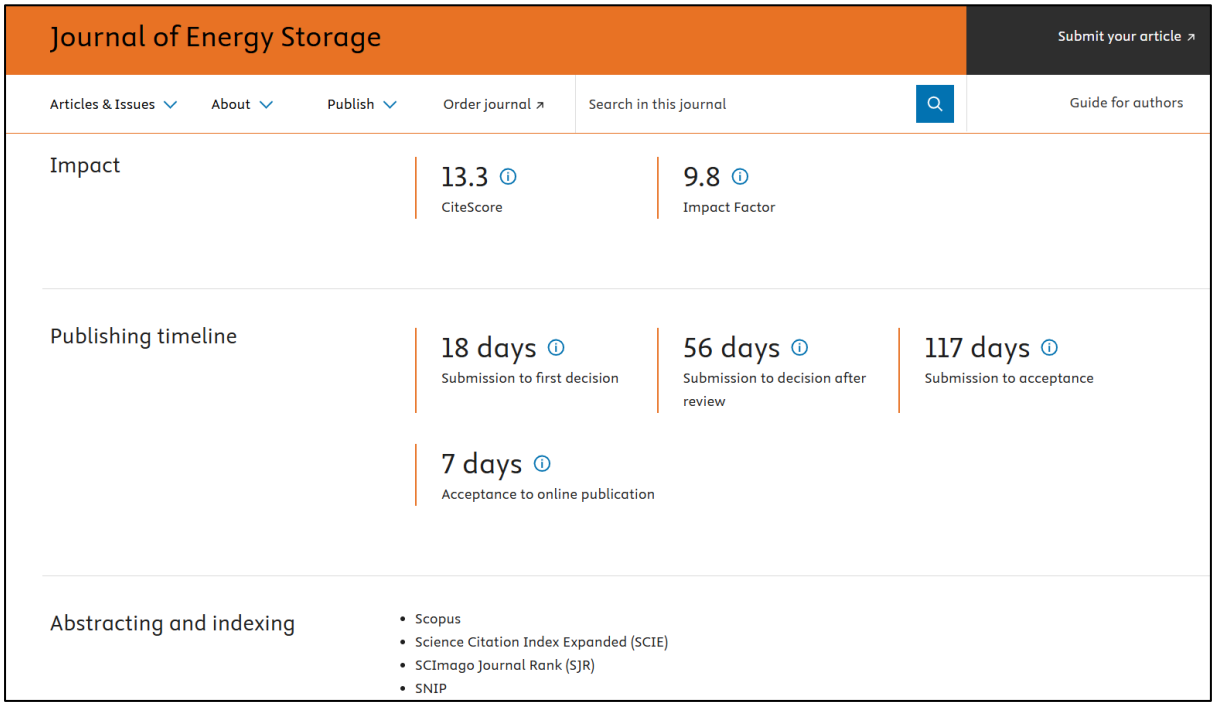

6.9 Master Journal Listing on Clarivate